Applied Physics Letters

RESEARCH ARTICLE | JANUARY 10 2024

Compact module for complementary-channel THz pulse slicing

Brad D. Price ; Antonín Sojka ; Nikolay I. Agladze ; Mark S. Sherwin

Appl. Phys. Lett. 124, 021107 (2024)
https://doi.org/10.1063/5.0180412

AIP Publishing

Applied Physics Letters ARTICLE pubs.aip.org/aip/apl

Compact module for complementary-channel THz pulse slicing

Cite as: Appl. Phys. Lett. **124**, 021107 (2024); doi: 10.1063/5.0180412
Submitted: 9 October 2023 · Accepted: 15 December 2023 ·
Published Online: 10 January 2024

Brad D. Price,[1,2,a)] Antonín Sojka,[1,2] Nikolay I. Agladze,[1,2] and Mark S. Sherwin[1,2,a)]

AFFILIATIONS

[1]Department of Physics, University of California, Santa Barbara, California 93106, USA
[2]Institute for Terahertz Science and Technology, University of California, Santa Barbara, California 93106, USA

[a)]**Authors to whom correspondence should be addressed:** bdprice@ucsb.edu and sherwin@ucsb.edu

ABSTRACT

We present a modular quasi-optical pulse slicer designed for use at terahertz (THz) frequencies. Given a quasi-cw input, the two outputs of a module are (1) a pulse with programmable duration and (2) its complement. The quasi-optical design incorporates a laser-driven silicon switch at Brewster's angle to the incoming THz beam, which limits undesired reflections before the switch is activated such that THz power is only transmitted when the switch is "on." An "off" switch ensures that no power is leaked after the pulse and that the switching profile is sharp. The slicer's small footprint ($0.048 \times 0.072 \times 0.162\ m^3$) and small insertion loss (1.2 dB at 320 GHz) as well as high switching efficiency (~70%) allows modules to be stacked to create multiple pulses. The output channel that is not used for experiments can be used for concurrent analysis of beam parameters. Stacking modular assemblies will enable more complex sequences of kW-level pulses than are currently achievable for applications including free-electron-laser or gyrotron-powered pulsed electron spin resonance at high magnetic fields.

High power, narrow band terahertz (0.1–10 THz) waves are crucial for heating plasmas in fusion reactors,[1,2] wireless communications with ultra-high data rates,[3–5] radar with millimeter-range spatial resolution,[6,7] electron beam accelerators,[8,9] and coherent manipulation of quantum states.[10,11] For all of these applications, complex THz waveforms are desirable; traveling-wave-tube and gyrotron amplifiers are under development to create such waveforms, but scaling them to high frequencies is challenging. Laser-generated narrow band waveforms may be used to produce high-power THz pulses, but the output bandwidth is still larger than 1 GHz.[9] Complex, narrow band THz waveforms can be, in principle, generated by modulating nearly monochromatic quasi-continuous wave sources. Examples of sources with kW power and sub-MHz bandwidths include free electron lasers (FELs) and gyrotron oscillators.[12–16]

The leading technique for modulating such waveforms uses laser-driven semiconductor switches (LDSS), where the optical excitation of a semiconducting wafer creates a high-carrier-density surface from what is otherwise a transparent material: reflectances of up to 90% have been reported for silicon[17,18] and gallium arsenide[18–22] substrates for switching powers up to nearly 1 MW.[23] Electronic modulation of such high power THz sources is also possible, but it is complicated by the low damage threshold of such modulators.[24]

An important application for high contrast pulse modulation is high field electron spin resonance (ESR), where even a small fraction of leaked pulse power reduces spectroscopic resolution.[25,26] ESR is an immensely powerful and sensitive spectroscopic tool that takes advantage of the Zeeman effect—electronic energy levels split by an applied magnetic field may be probed with electromagnetic radiation and can provide unique access to short- and long-range interactions between spins across a broad range of host materials.[25,27] In recent decades, ESR at frequencies above 95 GHz (3.5 T for $g \approx 2$) has grown in popularity because spectral resolution is greater, new phenomena can be accessed, and the increased polarizability of electrons can be transferred to nuclei to enhance the signal strength of high field nuclear magnetic resonance spectroscopy through dynamic nuclear polarization (DNP).[27–32] More specifically, pulsed ESR offers the opportunity to obtain spin–lattice and spin–spin relaxation times as well as resolve small spin–spin couplings.[33] It is crucial for an ESR pulse modulator to have sufficiently low power transmission in the off state to avoid undesirable induced magnetization. Since the flip angle, α, is proportional to $B_1 \propto \sqrt{P_{mw}}$ and the duration of the applied field,[33] this means that the time integral of the leaked microwave magnetic field in the off-state must be much less than that of the pulses:

$$\sqrt{P_l}t_l \ll \sqrt{P_p}t_p, \tag{1}$$

where P is the power, t is the time, and the indices l and p represent "leaked power" and "pulse power," respectively. In addition, it is of

course desirable to have maximal transmission in the on state in order to maximize the flip-angles that can be achieved in a given pulse.

A typical pulsed ESR experiment requires more than one pulse and the ability to control the relative phase in a sequence of pulses.[34] An LDSS apparatus that is capable of slicing up to two pulses from the output of an FEL, with the ability to control relative phases, has enabled FEL-powered ESR experiments, including free induction decay, Hahn echo, and spin–lattice relaxation time measurements in select systems.[34,35] However, pulse sequences of *more* than two pulses are typically desirable for pulsed ESR spectroscopy, and it is challenging to scale the existing pulse slicer design to more than two pulses due to spatial requirements. Furthermore, all pulse slicers reported to date have dumped the beam energy that is outside the pulse timings into an absorber to minimize standing waves and spectrometer ringdown. This dumped "complementary" beam is, thus, wasted in existing pulse slicer designs.[23,26,35]

The existing pulse slicing configuration as used for FEL-ESR at the Institute for Terahertz Science and Technology is described in the supplementary material Sec. I and shown in Fig. S1. The configuration was designed to ensure that all "on" switches were at Brewster's angle and in the same plane as the rest of the quasi-optics. This Brewster's angle setup has close to zero off-state transmission (<-60 dB) and is capable of producing one ($<1\,\mu$s) or two (one 1–20 ns, the other 1–40 ns) sharp pulses from a 1 μs FEL pulse.[35] Such a design has a very large footprint to generate only two pulses: one full optical table ($1.2 \times 2.4\,\mathrm{m}^2$) is required for optical components and another is required for the high-power (~100 mJ) Nd:YAG lasers and physical delay stages used for rise-and-fall timing manipulation. The large footprint and many optical components required (both visible and THz) also make the design prone to misalignment and imperfect coupling, which reduces the sharpness of the generated pulses as well as the peak ESR pulse power that can be achieved. Furthermore, the large footprint requires the use of high-density polyethylene THz lenses in order to preserve the input beam radius; however, such lenses also introduce partially reflective, normal-incidence surfaces that cause standing waves and increase spectrometer dead time through ringdown. Eliminating ringdown also requires that the complementary quasi-cw beam must be dumped into a THz absorber.

In this article, we present a modular pulse slicing design in which modules can be stacked in sequence to slice an arbitrary number of pulses from a THz quasi-continuous wave (cw) Gaussian beam. It is frequency agile, as well as cheaper by an order of magnitude, more robust, and approximately 30 times smaller than previous designs.[35] The modular design provides two outputs: the "additive" channel that contains the desired pulses, and—unique to this design—its complementary "subtractive" channel, which contains the complement of the sliced pulses. The subtractive channel—which has been dumped in previous pulse slicers—can be used as an input to a subsequent module to slice additional pulses, or concurrently measure beam parameters, such as power and phase.

The design incorporates parabolic mirrors ($f = 50.8$ mm, 35-644, Edmund Optics, Inc., NJ, USA) that focus the beam onto a silicon wafer and subsequently image the input beam to the output (see Fig. 1). This design has two qualities that assist in minimizing off-state reflection by the silicon wafer, which is crucial for pulsed ESR: incoming THz is directed toward the silicon switches at Brewster's angle ($n_{Si} = 3.4175$, $\theta_B = 73.69°$, Dai *et al.*[36]) and the modular assembly

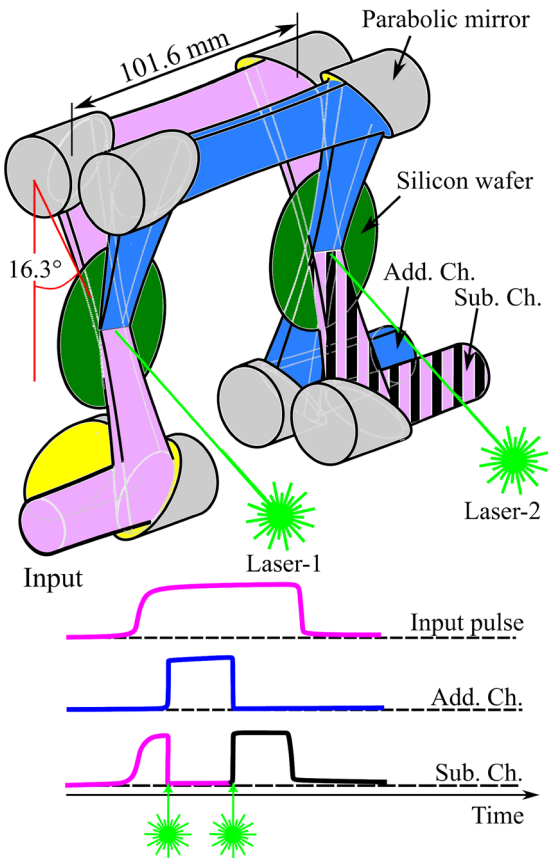

FIG. 1. Quasi-optics incorporated in one modular pulse slicer assembly. Parabolic mirrors focus collimated incoming THz waves (pink) onto a 50.8 mm diameter silicon wafer at Brewster's angle. Depending on switch state, the THz waves are either transmitted (pink) or reflected (blue) at the first switch. Similarly, pulses are either transmitted (pink and blue) or reflected (black) by the second switch. As shown in the timing diagram (bottom), during slicing, pink is output first, then blue, and finally black. A pulse (~3.8 mm beam diameter) from a 532 nm diode-pumped laser incident on the silicon wafer (in this figure, illumination is from the right-hand side of both wafers) promotes electrons into the conduction band and switches silicon from transmissive-to-reflective to THz for the duration of the lifetime of the carriers. Eight parabolic mirrors and two silicon wafers (as shown) constitute one pulse slicing assembly.

also allows silicon wafers of optimal thickness—such that front and back surface reflections at the silicon wafer destructively interfere—to be inserted by a stepper motor when input beam frequency is changed (see the supplementary material Sec. II A).

Off-state reflection can be caused by cross-polarization as a result of reflection by the curved surface of the parabolic mirrors[37] and the divergence of the Gaussian beam near its waist, which causes the edges of the beam to have incident angles that are different from its center.[38] Following Murphy, we estimate that 0.4% of the power in an incident Gaussian beam that is *p*-polarized to avoid reflection by a Si wafer at Brewster's angle is converted to *s*-polarized, which can be reflected at Brewster's angle (see the supplementary material Sec. II B 1). Doty *et al.*[39] showed that precisely tuning the wafer thickness can result in an additional 30 dB suppression of off-state reflections associated with both Gaussian beam divergence and polarization conversion.

Off-axis reflection by a parabolic mirror also causes a distortion that shifts the center of the Gaussian beam relative to its propagation axis.[37] However, since the 532 nm excitation pulse can be positioned to maximize overlap with the THz beam, this shift can be compensated for at the wafer surface. In the modular configuration presented here, the second parabolic mirror of each pair corrects for the distortion and reduces it to negligible levels at the output, as is discussed in Murphy.[37]

Figure 1 demonstrates the operation of a pulse slicing assembly, made up of two pulse slicing modules, to generate one pulse. The input THz beam (pink) is reflected by a parabolic mirror and subsequently passes through a silicon wafer (dark green) into the subtractive channel output. Upon activation of this wafer using laser-1, the input beam is reflected by the front surface of the wafer and directed into the additive channel (blue), while the subtractive channel is turned off. Each channel is collimated using its own parabolic mirror, producing two beams that match the original input beam's size and profile. These beams are used as inputs for the second module and the entire process is repeated. When laser-2 activates the second wafer, the beam in the additive channel is directed into the subtractive channel (now black), which turns off the additive channel and leaves a sharp pulse behind (see Fig. 1, bottom). Additional pulses can be generated using the output of the subtractive channel as the input for subsequent modules. A matrix formulation for the fields output by an arbitrary number of stacked modules is presented in the supplementary material Sec. II C and a simulation of their output powers is shown in the supplementary material Fig. S3.

A pulse slicing assembly is illustrated in Fig. 2; the largest components are two diode-pumped 532 nm lasers (VRN20-50-G, Lumibird Photonics, FR) that are used to drive the silicon switches. 532 nm lasers were chosen for optical excitation due to the maturity of their technology: diode-pumped lasers with small form factors are able to produce significant power at this wavelength and their photon energies are sufficiently high (larger than the bandgap of Si, $\lambda_{ex} < hc/E_{g,Si} = hc/1.13\,\text{eV} = 1.1\,\mu\text{m}$, Bludau *et al.*[40]). These lasers, in conjunction with the modules' housing and optics for laser beam expansion, are securely mounted onto a baseplate. Both 532 nm laser beams are reflected and expanded by a 9.5 mm focal length concave spherical mirror (CM127-010-G01, Thorlabs, Inc., NJ, USA): beam expansion ensures the overlap of THz and laser beam profiles on the silicon wafer's surface. Individual modules (highlighted in red in Fig. 2) were constructed from CNC-milled (CNC track precision 2.5 μm) aluminum housing that was designed to fix all quasi-optical components in place and minimize positioning errors (see the photograph of constructed test assembly in the supplementary material Fig. S4).

Each pulse slicer assembly (consisting of two modules) is designed to generate a single pulse. Because of its small footprint, additional assemblies could be stacked to generate more than two pulses (outlined in Fig. 2), and a protective enclosure could easily be employed to increase eye safety and reduce scattered laser light.

The capabilities of complementary-channel modular pulse slicer design were demonstrated using a 320 GHz source-and-detector test setup (VDI-S027 source, Virginia Diodes, Inc., VA, USA; AC-coupled quasi-optical detector, 3DL 12C LS2500 A2, ACST gmbH, DE) and two $279 \pm 25\,\mu$ m float-zone, high-resistivity, $\langle 111 \rangle$ undoped silicon wafers (Virginia Semiconductor, Inc., VA, USA). The wafer thickness was optimized such that front and back surface reflections at 320 GHz destructively interfered when oriented at Brewster's angle, using

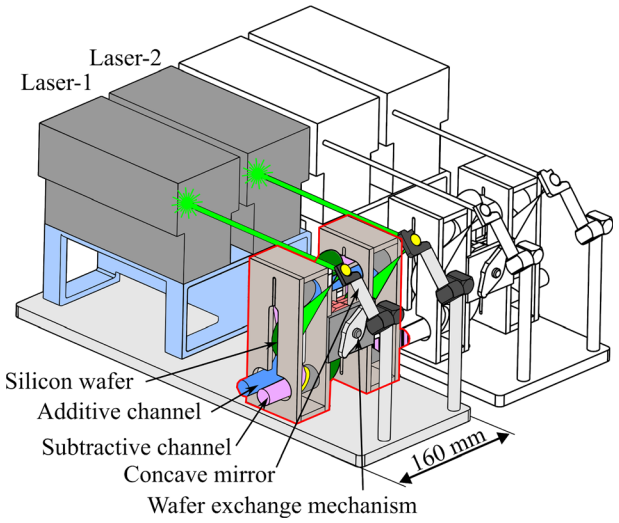

FIG. 2. Modular pulse slicing assembly. The arrangement of mirrors, silicon wafers, and THz Gaussian beams (as depicted in Fig. 1) is integrated within two pulse slicer modules, which are highlighted by the red outlines. The overall assembly involves two 25 mJ lasers that both emit a 9 ns 532 nm pulse, ~ 3.8 mm in diameter, that is expanded beyond the focal length (9.5 mm) of a spherical concave mirror to fully cover the face of the silicon wafer (and incident THz Gaussian beam) inside each module. The pulse slicer module precisely aligns four parabolic mirrors with a silicon wafer at Brewster's angle using slip- and press-fit pairs of dowel pin holes. The assembly's stackable nature is visually depicted in a black and white illustration—the configuration shown would be used to make two sharp pulses from a high power quasi-cw beam.

$$T = \frac{m\lambda}{2\left(\sqrt{n_{\text{Si}}^2 - n_{\text{air}}^2 \sin^2\theta_i}\right)} \tag{2}$$

from Doty *et al.*[39] after substitution using Snell's law, where T is the wafer thickness and m is an integer that represents the interference order. The AC-coupled detector, with an amplifier bandwidth of 4 MHz–4 GHz, converted 320 GHz power into a voltage. Pulse slicing experiments were done in either "cw" mode, where a pulse was directly sliced from a low-power cw beam, or "stepped" (convolution) mode, where a 20 ns pulse was stepped through the slicing timing. In both modes, the 320 GHz power was approximately 100 μW.

Figure 3 demonstrates sliced pulses with durations between 1 and 50 ns generated by two lasers and two wafers. The rise and fall times of these edges are currently limited by the 9 ns pulse length of the laser used (depicted in gray in Fig. 3). Shorter pulses with faster rise and fall times could be achieved by activating the silicon switch with picosecond or even femtosecond laser pulses.[41,42] Recorded pulse profiles are distorted due to the AC-coupling of the detector, but the detector's fast response was able to capture the slopes of the rising and falling edges.

To avoid the limitations of the AC-coupled quasi-optical detector, we also measured the transfer function of the modular pulse slicer by stepping the timing of a 20 ns, 320 GHz close-to-square probe pulse with respect to the timing of laser pulses 1 and 2. This method returns a convolution of the transfer function and probe pulse with rising and falling edges less steep than a pulse sliced from a cw beam (simulation of the convolution effect is shown in the supplementary material Fig. S5).

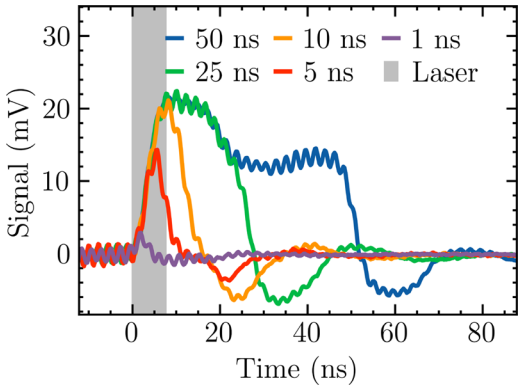

FIG. 3. Pulses sliced from cw 320 GHz Gaussian beam. The delays between on and off switch timings are shown in the legend. Peak power remains consistent down to approximately 10 ns pulses, below which it is reduced. Below 10 ns on-and-off delay, the pulse length of the laser ($\sim$ 9 ns,[43] shown by the gray vertical rectangle at $t = 0$) does not allow for the full 25 mJ to be deposited onto the wafer before the pulse is switched off. The deviations from square temporal profiles are due to the AC coupling of the detector. The fine structure (with fringe period of 2.2 ns) is attributed to electromagnetic interference that manifests when the 532 nm laser is fired. Experiments were repeated at 20 Hz. Exponential continuous averaging was used, with an effective time constant of 1.55 s, corresponding to 31 oscilloscope traces at 20 Hz (see the supplementary material Sec. III for further explanation of exponential averaging).

The additive and subtractive outputs of complementary-channel pulse slicing are shown in Fig. 4, which highlights the temporal flexibility of the modular design. Figure 4(a) shows 25 and 100 ns pulses with peak reflectances around 70%. Figure 4(b) shows the power returned by the complementary subtractive channel; the power in this channel can be used to create additional pulses by stacking modules. The maximum power of each subsequent pulse n is given by $P_n = P_0 R^{2n-1}$, where R is the peak reflectance of the wafer.

The modular pulse slicer relies on the long recombination time of photo-excited electrons and holes in silicon. As shown in Fig. 4, for the wafers used, the reflectance remains substantial for 10 μs, and over the sub-μs duration of a typical FEL-ESR pulse sequence (<1 μs, shown in red in Fig. 5), decays by less than 10%. The specific shape of the decay depends on the charge carriers' surface recombination, Auger lifetime, diffusion, and the Shockley–Read–Hall recombination due to impurities.[23,44] Recombination due to surfaces and impurities may be mitigated in the future by adapting methods and materials developed for silicon photovoltaics.[45]

The results demonstrate the feasibility of a frequency-agile quasi-optical pulse slicing module for slicing short (>1 ns) pulses from a cw or quasi-cw THz source. The modular design vastly reduces the required space compared to the most sophisticated previous design and can slice pulses with a $0.048 \times 0.072\ \mathrm{m}^2$ footprint rather than a large fraction of a $1.2 \times 2.4\ \mathrm{m}^2$ optical table.[35] The modules can also be stacked together to slice as many pulses as necessary, which will enable three-pulse echo-detected inversion recovery ESR experiments, for example. The timings of the pulse edges are set entirely electronically and do not require a physical delay stage that would cap the maximum pulse length. Additionally, this modular design requires no custom optics and can be almost entirely constructed with three CNC-milled parts.

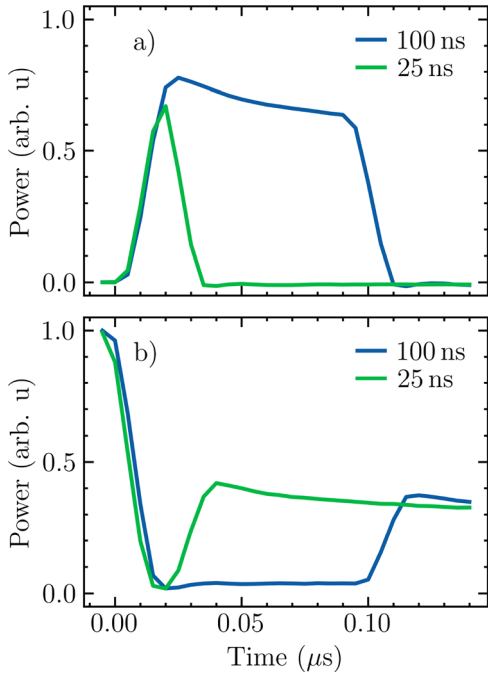

FIG. 4. Sliced pulses of 25 and 100 ns. Pulses shorter than 25 ns, while possible, suffer significant distortion due to convolution with the 20 ns probe pulse. Exponential continuous averaging was used, with an effective time constant of 1.55 s, corresponding to 31 oscilloscope traces at 20 Hz. (a) Additive channel that makes up the sequence of pulses. Power is normalized to the transmitted power with both lasers off. (b) Subtractive channel that subsequent pulses are sliced from. Power is normalized to the transmitted power with both lasers off. Each data point represents the integrated power of a 20 ns THz pulse that was swept through the laser timing. The recorded data are a convolution of the slice timing with the probe pulse and results in a less sharp recorded profile than that shown in Fig. 3.

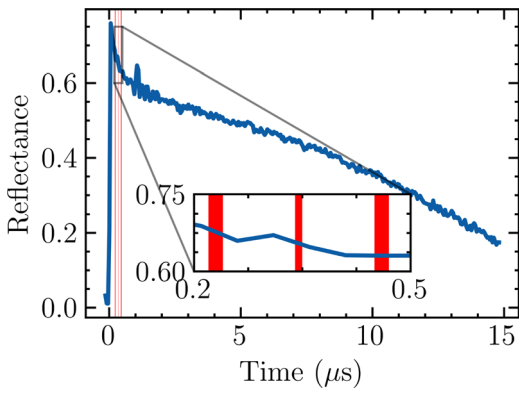

FIG. 5. Reflectance of a single silicon wafer after excitation by a 25 mJ, 532 nm laser pulse. Power in the additive channel was measured by sweeping a 20 ns THz pulse in time across the laser pulse timing and integrating the total power of the THz pulse. Reflectance (solid blue) was calculated by dividing the power measured in the additive channel by the power in the subtractive channel when the switch was not activated. Experiments were repeated at 20 Hz. Exponential continuous averaging was used, with an effective time constant of 1.55 s, corresponding to 31 oscilloscope traces at 20 Hz. (Inset) Reflectance between 0.2 and 0.5 μs overlaid with a typical echo-detected inversion recovery pulsed ESR sequence (pulse timings shown with red vertical bars).

The insertion loss of the subtractive channel of the pulse slicer was measured to be 1.2 dB at 320 GHz, which was obtained by comparing the power into and out of the slicing assembly test setup, which consisted of three pulse slicing modules. This loss can be attributed to four factors: (1) imperfect quasi-optical coupling that may be present due to alignment of optical components, imperfections in mirror manufacturing, and small off-axis parabolic mirror distortions;[37,46,47] (2) spatial filtering of the THz beam by the pairs of off-axis parabolic mirrors; (3) ohmic losses at the metallic surfaces of the mirrors; and (4) losses at the semiconducting wafer face due to portions of the beam that are not at Brewster's angle.

(1) *Imperfect quasi-optical coupling:* Parabolic mirror distortions, resulting from off-axis reflection of a Gaussian beam, convert small amounts of power from the fundamental mode to higher-order modes, resulting in small power losses from the fundamental mode. According to Murphy,[37] a pair of mirrors in the reported pulse slicer configuration should reduce this distortion to negligible amounts. An upper bound on losses due to mode conversion is, thus, the loss from one mirror without compensation, which we estimate, following Murphy,[37] to be $\eta_d = 0.002$ at 320 GHz (see the supplementary material Sec. II B 2). This implies a maximum loss of 0.0085 dB by each mirror pair, totaling 0.026 dB through the three module test setup.
(2) *Spatial filtering of the THz beam:* The pulse slicer was designed for slicing a TEM_{00} beam; higher order modes that can appear in an input beam due to imperfections in quasi-optics are larger than the fundamental TEM_{00} mode and are thereby filtered by the pairs of parabolic mirrors and contribute to the measured insertion loss.[48]
(3) *Ohmic loss:* The estimated ohmic loss on a metallic mirror surface was around 0.2%;[46,49,50] the loss as a result of seven mirrors in series totals approximately 0.06 dB. The seven mirrors consisted of the six parabolic mirrors incorporated in three modules, and one flat mirror in place of a third silicon wafer that was used to facilitate switching between detected output channel.
(4) *Losses due to deviations from Brewster's angle:* The losses as a result of divergence of the beam at the focus and slight cross-polarization are assumed to be negligible in this setup because the wafer thickness was tuned such that reflections from the front and back surfaces destructively interfered. However, an upper bound of the cross-polarization losses can be estimated by assuming that all *s*-polarized THz radiation incident on the wafer is lost through reflection, similar to the treatment for distortion losses. As calculated previously (see the supplementary material Sec. II B 1), cross-polarization creates a fractional loss of $\eta_d = 0.004$ input *p*-polarized beam power at each semiconducting wafer interface, leading to a total loss of 0.034 dB through one assembly.[37,48]

Under these assumptions, the total loss through the test bench setup is approximately 0.12 dB, which is much smaller than the observed loss. The rest of the insertion loss (approximately 1.1 dB) can be attributed to alignment and mirror machining imperfections. The finite thickness of the semiconducting wafer necessarily contributes some misalignment in one of the two channels that cannot be accounted for due to the need for a variety of wafer thicknesses. In total, 1.2 dB insertion loss is acceptable when working with kW-power THz beams.

The insertion loss of the additive channel is dominated by the peak reflectance of the semiconducting wafer, with additional losses from imperfect quasi-optical coupling, spatial filtering, and ohmic losses, comparable to those of the subtractive channel. Figure S6 of the supplementary material depicts a simulation of a diameter that encloses 99% of the encircled energy for a selection of DNP frequencies and demonstrates that frequencies higher than 240 GHz will propagate without issue. Below 240 GHz, more power will be lost because the circle enclosing 99% encircled energy of the Gaussian profile falls outside the diameter of the silicon wafer. Below 150 GHz, the circle enclosing 99% encircled beam energy also falls outside the input diameter of the parabolic mirrors.

In this paper, we present quasi-optical pulse slicing modules that are capable of slicing flexible pulse durations over a wide range of frequencies (>240 GHz). The design is cost-efficient, uses commercially available mirrors, and can produce pulses of arbitrary duration (>1 ns) from a cw or quasi-cw THz beam. It is modular and stackable, allowing *n* pulses to be created by simply stacking 2*n* modules in series, and returns the additive channel and its complement, enabling concurrent analysis of beam parameters. The capabilities demonstrated here make the pulse slicer highly flexible and useful for a broad range of spectroscopic applications including FEL-[35] or gyrotron-[26] powered pulsed ESR and DNP.

See the supplementary material for additional information on the pulse slicer design and current FEL-ESR pulse slicer, as well as accompanying figures.

The authors thank Dr. Seamus D. O'Hara for his assistance designing and aligning the quasi-optical testing setup. They also gratefully acknowledge funding from the NSF through DMR 2117994.

AUTHOR DECLARATIONS

Conflict of Interest

B.D.P., A.S., N.I.A., and M.S.S. have patent pending.

Author Contributions

Brad D. Price: Conceptualization (supporting); Data curation (lead); Formal analysis (supporting); Investigation (equal); Methodology (equal); Software (lead); Validation (equal); Visualization (equal); Writing – original draft (lead); Writing – review & editing (equal). **Antonín Sojka:** Conceptualization (supporting); Data curation (supporting); Formal analysis (supporting); Investigation (equal); Methodology (equal); Software (supporting); Validation (equal); Visualization (equal); Writing – original draft (supporting); Writing – review & editing (equal). **Nikolay I. Agladze:** Conceptualization (lead); Formal analysis (lead); Investigation (supporting); Methodology (supporting); Supervision (supporting); Writing – original draft (supporting); Writing – review & editing (equal). **Mark S. Sherwin:** Conceptualization (supporting); Funding acquisition (lead); Investigation (supporting); Project administration (lead); Supervision (lead); Writing – original draft (supporting); Writing – review & editing (equal).

DATA AVAILABILITY

The data that support the findings of this study are openly available in Zenodo at http://doi.org/10.5281/zenodo.8388175, Ref. 51.

REFERENCES

[1]C. Paoloni, D. Gamzina, L. Himes, B. Popovic, R. Barchfeld, L. Yue, Y. Zheng, X. Tang, Y. Tang, P. Pan, H. Li, R. Letizia, M. Mineo, J. Feng, and N. C. Luhmann, IEEE Trans. Plasma Sci. **44**, 369 (2016).
[2]T. Kariya, T. Imai, R. Minami, K. Sakamoto, Y. Oda, R. Ikeda, T. Shimozuma, S. Kubo, H. Idei, T. Numakura, K. Tsumura, Y. Ebashi, M. Okada, Y. Nakashima, Y. Yoshimura, H. Takahashi, S. Ito, K. Hanada, K. Nagasaki, M. Ono, T. Eguchi, and Y. Mitsunaka, Nucl. Fusion **57**, 066001 (2017).
[3]R. Kersting, G. Strasser, and K. Unterrainer, Electron. Lett. **36**, 1156 (2000).
[4]S. Koenig, D. Lopez-Diaz, J. Antes, F. Boes, R. Henneberger, A. Leuther, A. Tessmann, R. Schmogrow, D. Hillerkuss, R. Palmer, T. Zwick, C. Koos, W. Freude, O. Ambacher, J. Leuthold, and I. Kallfass, Nat. Photonics **7**, 977 (2013).
[5]M. A. Akkaş, Wireless Networks **25**, 145 (2019).
[6]K. B. Cooper, R. J. Dengler, N. Llombart, B. Thomas, G. Chattopadhyay, and P. H. Siegel, IEEE Trans. Terahertz Sci. Technol. **1**, 169 (2011).
[7]X. Zhang, T. Chang, Z. Wang, and H.-L. Cui, IEEE Access **8**, 144259 (2020).
[8]E. A. Nanni, W. R. Huang, K.-H. Hong, K. Ravi, A. Fallahi, G. Moriena, R. J. Dwayne Miller, and F. X. Kärtner, Nat. Commun. **6**, 8486 (2015).
[9]D. Zhang, M. Fakhari, H. Cankaya, A.-L. Calendron, N. H. Matlis, and F. X. Kärtner, Phys. Rev. X **10**, 011067 (2020).
[10]P. Salén, M. Basini, S. Bonetti, J. Hebling, M. Krasilnikov, A. Y. Nikitin, G. Shamuilov, Z. Tibai, V. Zhaunerchyk, and V. Goryashko, Phys. Rep. **836–837**, 1–74 (2019).
[11]J. B. Costello, S. D. O'Hara, Q. Wu, D. C. Valovcin, L. N. Pfeiffer, K. W. West, and M. S. Sherwin, Nature **599**, 57 (2021).
[12]V. Flyagin, A. Gaponov, I. Petelin, and V. Yulpatov, IEEE Trans. Microwave Theory Tech. **25**, 514 (1977).
[13]N. Kumar, U. Singh, T. P. Singh, and A. K. Sinha, J. Fusion Energy **30**, 257 (2011).
[14]M. Hruszowiec, K. Nowak, B. Szlachetko, M. P. Grzelczak, W. Czarczyński, E. F. Pliński, and T. Więckowski, J. Telecommun. Inf. Technol. **2**, 18 (2017).
[15]G. Ramian, Nucl. Instrum. Methods Phys. Res., Sect. A **318**, 225 (1992).
[16]P. G. O'Shea and H. P. Freund, Science **292**, 1853 (2001).
[17]S. Takahashi, G. Ramian, and M. S. Sherwin, Appl. Phys. Lett. **95**, 234102 (2009).
[18]G. Li, E. L. Claveau, S. K. Jawla, S. C. Schaub, M. A. Shapiro, and R. J. Temkin, IEEE Trans. Terahertz Sci. Technol. **13**, 354 (2023).
[19]S. Kutsaev, B. Jacobson, A. Smirnov, T. Campese, V. Dolgashev, V. Goncharik, M. Harrison, A. Murokh, E. Nanni, J. Picard, M. Ruelas, and S. Schaub, Phys. Rev. Appl. **11**, 034052 (2019).
[20]M. L. Kulygin, IEEE Trans. Terahertz Sci. Technol. **9**, 186 (2019).
[21]G. G. Denisov, A. V. Palitsin, D. I. Sobolev, V. I. Belousov, I. A. Gorbunov, O. V. Kulagin, S. V. Morozov, A. A. Murzanev, A. N. Stepanov, and M. Y. Glyavin, in 46th International Conference on Infrared, Millimeter and Terahertz Waves (IRMMW-THz), 2021.
[22]G. Denisov, A. Palitsin, D. Sobolev, V. Parshin, and M. Glyavin, in 24th International Vacuum Electronics Conference (IVEC), 2023.
[23]J. F. Picard, S. C. Schaub, G. Rosenzweig, J. C. Stephens, M. A. Shapiro, and R. J. Temkin, Appl. Phys. Lett. **114**, 164102 (2019).
[24]S. Hawasli, S. Nadri, L. Xie, and R. M. Weikle, in *IEEE MTT-S International Microwave Symposium (IMS)* (IEEE, 2016).
[25]J. A. Weil and J. R. Bolton, *Electron Paramagnetic Resonance: Elementary Theory and Practical Applications* (John Wiley & Sons, 2007).
[26]S. Mitsudo, C. Umegaki, K. Hiiragi, M. Narioka, Y. Fujii, and Y. Tatematsu, in 41st International Conference on Infrared, Millimeter, and Terahertz Waves (IRMMW-THz), 2016.
[27]A. Abragam and M. Goldman, Rep. Prog. Phys. **41**, 395 (1978).
[28]A. Schnegg, *eMagRes* (John Wiley & Sons, Ltd, 2017), pp. 115–132.
[29]L. R. Becerra, G. J. Gerfen, R. J. Temkin, D. J. Singel, and R. G. Griffin, Phys. Rev. Lett. **71**, 3561 (1993).
[30]P. Neugebauer, J. G. Krummenacker, V. P. Denysenkov, G. Parigi, C. Luchinat, and T. F. Prisner, Phys. Chem. Chem. Phys. **15**, 6049 (2013).
[31]V. K. Michaelis, R. G. Griffin, B. Corzilius, and S. Vega, *Handbook of High Field Dynamic Nuclear Polarization* (John Wiley & Sons, 2019).
[32]Y. Zhao, H. El Mkami, R. I. Hunter, G. Casano, O. Ouari, and G. M. Smith, Commun. Chem. **6**(1), 171 (2023).
[33]S. Stoll, *eMagRes* (John Wiley & Sons, Ltd, 2017), pp. 23–38.
[34]C. Blake Wilson, S. Aronson, J. A. Clayton, S. J. Glaser, S. Han, and M. S. Sherwin, Phys. Chem. Chem. Phys. **20**, 18097 (2018).
[35]S. Takahashi, L.-C. Brunel, D. T. Edwards, J. van Tol, G. Ramian, S. Han, and M. S. Sherwin, Nature **489**, 409 (2012).
[36]J. Dai, J. Zhang, W. Zhang, and D. Grischkowsky, J. Opt. Soc. Am. B **21**, 1379 (2004).
[37]J. A. Murphy, Int. J. Infrared Millimeter Waves **8**, 1165 (1987).
[38]Q. Li and R. J. Vernon, IEEE Trans. Antennas Propag. **54**, 3449 (2006).
[39]M. F. Doty, B. E. Cole, B. T. King, and M. S. Sherwin, Rev. Sci. Instrum. **75**, 2921 (2004).
[40]W. Bludau, A. Onton, and W. Heinke, J. Appl. Phys. **45**, 1846 (1974).
[41]C. Rolland and P. B. Corkum, J. Opt. Soc. Am. B **3**, 1625 (1986).
[42]F. A. Hegmann and M. S. Sherwin, *Millimeter and Submillimeter Waves and Applications III* (SPIE, 1996), Vol. 2842, pp. 90–105.
[43]Lumibird, "Viron: Compact pulsed diode-pumped Nd:YAG laser" (2021), available at https://www.quantel-laser.com/tl_files/client/docs_produits/Viron_Specs_052021REVF.pdf.
[44]R. Häcker and A. Hangleiter, J. Appl. Phys. **75**, 7570 (1994).
[45]T. Niewelt, M. Selinger, N. E. Grant, W. Kwapil, J. D. Murphy, and M. C. Schubert, J. Appl. Phys. **121**, 185702 (2017).
[46]Edmund Optics, "25.4 × 50.8 mm EFL 90° bare gold 100Å off-axis parabolic mirror" (2023), available at https://www.edmundoptics.com/p/254-x-254mm-pfl-90-off-axis-parabolic-bare-gold-mirror/33554/.
[47]T. J. Finn, N. Trappe, J. A. Murphy, and S. Withington, Infrared Phys. Technol. **51**, 351 (2008).
[48]P. F. Goldsmith, *Quasioptical Systems* (IEEE Press, New York, 1998).
[49]W. Kasparek, A. Fernandez, F. Hollmann, and R. Wacker, Int. J. Infrared Millimeter Waves **22**, 1695 (2001).
[50]E. A. Serov, V. V. Parshin, and G. M. Bubnov, IEEE Trans. Microwave Theory Tech. **64**, 3828 (2016).
[51]B. D. Price and A. Sojka (2023). "Dataset and code: Compact module for complementary-channel THz pulse slicing," Zenodo.